8-31-2020

Hypusination of Eif5a Regulates Cytoplasmic TDP-43 Aggregation and Accumulation in a Stress-Induced Cellular Model

Shayna Smeltzer
University of South Florida

Zainuddin Quadri
University of Kentucky, Zainuddin.Quadri@uky.edu

Abraian Miller
University of South Florida

Frank Zamudio
University of South Florida

Jordan Hunter
University of South Florida

Hypusination of Eif5a Regulates Cytoplasmic TDP-43 Aggregation and Accumulation in a Stress-Induced Cellular Model

Digital Object Identifier (DOI)
https://doi.org/10.1016/j.bbadis.2020.165939

Notes/Citation Information

Published in *Biochimica et Biophysica Acta (BBA)- Molecular Basis of Disease,* v. 1867, issue 1, 165939.

Authors

Shayna Smeltzer, Zainuddin Quadri, Abraian Miller, Frank Zamudio, Jordan Hunter, Nicholas J.F. Stewart, Sheba Saji, Daniel C. Lee, Dale Chaput, and Maj-Linda B. Selenica

BBA - Molecular Basis of Disease 1867 (2021) 165939

Contents lists available at ScienceDirect

BBA - Molecular Basis of Disease

journal homepage: www.elsevier.com/locate/bbadis

Hypusination of Eif5a regulates cytoplasmic TDP-43 aggregation and accumulation in a stress-induced cellular model

Shayna Smeltzer[a], Zainuddin Quadri[a,c], Abraian Miller[a], Frank Zamudio[a], Jordan Hunter[a], Nicholas J.F. Stewart[a], Sheba Saji[a], Daniel C. Lee[a,c], Dale Chaput[b], Maj-Linda B. Selenica[a,c,*]

[a] Department of Pharmaceutical Sciences, College of Pharmacy, University of South Florida, 12901 Bruce B. Downs Blvd, Tampa, FL 33612, USA
[b] Proteomics and Mass Spectrometry Core Facility, Florida Center of Excellence for Drug Discovery and Innovation (CDDI), University of South Florida, 3720 Spectrum Blvd, Suite 303, Tampa, FL 33612, USA
[c] Sanders-Brown Center on Aging, Department of Molecular and Cellular Biochemistry, College of Medicine, University of Kentucky, KY, USA

ARTICLE INFO

Keywords:
eIF5A
Hypusination
TDP-43
Cytoplasmic accumulation
Stress granule
Nuclear import
Proteinopathy

ABSTRACT

TAR DNA-binding protein 43 (TDP-43) is a nuclear RNA/DNA binding protein involved in mRNA metabolism. Aberrant mislocalization to the cytoplasm and formation of phosphorylated/aggregated TDP-43 inclusions remains the hallmark pathology in a spectrum of neurodegenerative diseases, including frontotemporal disorders and Alzheimer's disease. Eukaryotic Translation Initiation Factor 5A undergoes a unique post-translation modification of lysine to hypusine (K50), which determines eIF5A binding partners. We used a sodium arsenite-induced cellular stress model to investigate the role of hypusinated eIF5A (eIF5A^{HypK50}) in governing TDP-43 cytoplasmic mislocalization and accumulation in stress granule. Our proteomics and functional data provide evidence that eIF5A interacts with TDP-43 in a hypusine-dependent manner. Additionally, we showed that following stress TDP-43 interactions with eIF5A^{HypK50} were induced both in the cytoplasm and stress granules. Pharmacological reduction of hypusination or mutations of lysine residues within the hypusine loop decreased phosphorylated and insoluble TDP-43 levels. The proteomic and biochemical analysis also identified nuclear pore complex importins KPNA1/2, KPNB1, and RanGTP as interacting partners of eIF5A^{HypK50}. These findings are the first to provide a novel pathway and potential therapeutic targets that require further investigation in models of TDP-43 proteinopathies.

1. Introduction

The TDP-43 proteinopathies include a spectrum of neurodegenerative diseases where TDP-43 proteinopathy is present in 45% of cases of frontotemporal disorders (FTD)-TDP-43 subtype, and in 97% of patients with ALS with or without the cognitive impairment resembling FTD [1–3]. Recently, limbic-predominant age-related TDP-43 encephalopathy (LATE) was described as a common condition in patients 80 years or older [4]. To date, TDP-43 proteinopathies are defined by a nuclear loss-of-function (LOF) and cytoplasm toxic gain-of-function (GOF), both of which lead to the formation of TDP-43 cytoplasmic inclusions in distinct brain regions in patients [2,4,5]. Nuclear TDP-43 plays an important role in the regulation of mRNA splicing, metabolism, and transport, however the etiology of these mechanisms is less understood [5–7]. The pathological phenotype of GOF is characterized by cytoplasmic inclusions of TDP-43 containing abnormal ubiquitylated, phosphorylated, insoluble TDP-43 as well as truncated 25–35 kDa TDP-43 C-terminal fragments (CTFs), followed by vast neurodegeneration [2]. Interestingly, TDP-43 is incorporated into cytoplasmic stress granules (SGs) that have been robustly observed in ALS, FTD brain, and animal models [8–12]. The mechanism of nuclear to SG trafficking of TDP-43 is unknown, but the idea of SGs as early-sites for TDP-43 protein aggregation has been proposed [11].

Eukaryotic Translation Initiation Factor 5A (eIF5A) is a small, acidic protein that is highly conserved throughout eukaryotes. eIF5A is the only cellular protein that utilizes spermidine to modify lysine 50 (K50) to hypusine residue [hypusine-N-(4-amino-2-hydroxybutyl) lysine] [13]. Hypusination occurs via two subsequentially enzymatic events executed by deoxyhypusine synthase (DHS, rate-limiting enzyme) and deoxyhypusine hydroxylase (DOHH) [14]. Sequence conservation is especially high within the “hypusine loop”, underscoring the importance of this unusual protein modification throughout eukaryotic

* Corresponding author at: Sanders-Brown Center on Aging and Department of Molecular and Cellular Biochemistry, 422 Sanders-Brown Building, University of Kentucky College of Medicine, 800 S. Limestone St., Lexington, KY 40536, USA.
E-mail address: Maj-Linda.Selenica@uky.edu (M.-L.B. Selenica).

https://doi.org/10.1016/j.bbadis.2020.165939
Received 18 May 2020; Received in revised form 27 July 2020; Accepted 17 August 2020
Available online 31 August 2020

evolution [15]. Early studies underlined the role of hypusinated eIF5A ($eIF5A^{HypK50)\ in}$ translation initiation process [13] and served as bases for discovering $eIF5A^{HypK50}$ regulation of translation elongation of mRNAs involved in nuclear transport [16], mRNAs turnover [17], as well as posttranslational stress responses [18,19]. Further studies further suggested that acetylation of lysine 47 and 68 within the "hypusine loop" presents another mechanisms for regulation of eIF5A cellular localization and activity [20–22].

Despite studies shedding light on the importance of hypusination in a range of biological processes, a significant gap exists regarding the role of $eIF5A^{HypK50}$ in the neurobiological processes. A proteomic study demonstrated the first evidence of interactions of eIF5A with TDP-43 identifying TDP-43 binding to the N-terminal of eIF5A in a hypusine-dependent manner [23]. Another study suggested the role of eIF5A in unfolded protein response (UPR) and chaperone expression [24], conceivably implicating the eIF5A pathway in aberrantly folded protein responses. These findings provided the initial rationale for a plausible functional role of $eIF5A^{HypK50}$ in neurodegenerative diseases. Therefore, we aimed to investigate the role of $eIF5A^{HypK50}$ in TDP-43 proteinopathy focusing on the toxic GOF; cytoplasmic accumulation and aggregation, in several cellular models. We demonstrated that hypusinated eIF5A governs the TDP-43 sequestration to the cytoplasm and accumulation into the stress granule (SG) in sodium arsenite (SA) induced stress model. Importantly, we show that pharmacological inhibition of hypusination reduced TDP-43 cytoplasmic sequestration, phosphorylation, and aggregation as well as weakened the TDP-43 associations with $eIF5A^{HypK50}$ in a tetracycline regulatable TDP-43 HeLa isogenic cellular model [3]. We report that a reduction in hypusine levels did not affect the overall *de-novo* protein synthesis in this cellular model, suggesting that hypusination regulates mainly eIF5A-TDP-43 protein interactions. Lastly, proteomics and functional analysis identified nucleocytoplasmic transport cargo molecules; Ran, Karyopherin Subunit Alpha 1 and 2 (KPNA1/A2), and Karyopherin Subunit Beta 1(KPNAB1), as complex molecules of $eIF5A^{HypK50}$. Importantly, we demonstrated the advantages of the hypusination moiety as a novel therapeutic strategy against several features of the TDP-43 pathology in common dementias.

2. Material and methods

2.1. Cell culture and treatment

HeLa LAP-wtTDP-43 cells (gifted by Dr. DW. Cleveland, Ludwig Institute for Cancer Research, University of California at San Diego, La Jolla, CA, USA) were grown as described [3]. Briefly, HeLa cells were maintained in OptiMEM media (Gibco by Life Technologies, CA, USA, # 31985-070), 10% Heat-Inactivated Fetal Bovine Serum (HI-FBS, Sigma Aldrich, MO, USA, # F4135), and 1% Penicillin Streptomycin (Gibco by Life Technologies, CA, USA, # 15140122). LAP-wtTDP-43 cells were seeded in media containing 1 μg/mll tetracycline (tet, Sigma Aldrich, MO, USA, # 87128) for 24 h before treatment with 30 μM N1-guanyl-1,7-diaminoheptane for 72 h (GC7, Calbiochem, CA, USA, # 150333-69-0), followed by 0.5 mM sodium arsenite for 1 h (Ricca Chemical Company, TX, USA, # R7142000) (Supplementary Table 4). M17 cells were grown in OptiMEM, 10% HI-FBS, and 1% glutamax (Gibco by Life Technologies, CA, USA, # 35050061).

For the mutagenesis experiments, eIF5A and K47/50R-eIF5A plasmids (generously gifted from Dr. MH Park, Oral, and Pharyngeal Cancer Branch, National Institute of Dental and Craniofacial Research, National Institutes of Health, Bethesda, MD, USA) were transfected into Hek293T cells. Cells were grown to 70% confluency in DMEM media (Gibco by Life Technologies, CA, USA, # 11965092) supplemented with 10% Heat-Inactivated Fetal Bovine Serum (HI-FBS, Sigma Aldrich, MO, USA, # F4135) and 1% Penicillin Streptomycin (Gibco by Life Technologies, CA, USA, # 15140122). DMEM media was replaced with serum-deprived OptiMEM media (Gibco by Life Technologies, CA, USA, # 31985-070) and incubated at 37 °C for 20 min. The transfection reaction was performed as recommended by the manufacturer (Invitrogen by Thermo Fisher Scientific, USA, # 11668-019). Briefly, 1μg of plasmid was mixed in a 1:1.5 ratio with Lipofectamin™ 2000 Transfection Reagent in OptiMEM media and incubated at room temperature for 20 min before treatment. OptiMEM media was changed to complete DMEM media 7 h later. Cells were harvested 72 h post-transfection and prepared for Western blot.

2.2. AlamarBlue cell viability assay

HeLa cells were grown in 96-well plate at a maximum density of 100, 000 cells/well. 10 μl AlamarBlue (1: 10 dilution, # BUF012A, BioRad, CA, US) was added to each well and incubated for 1–4 h at 37 °C (pH 6.8–7.4). The fluorescence intensity was measured using BioTek Cytation 5.0 plate reader (530-560 nm) to measure cell respiration as an indicator for proliferation. Data are normalized to control and presented as percent change.

2.3. Site-directed mutagenesis

Site-directed mutagenesis was performed using QuickChange Site-Directed Mutagenesis kit (# 200518) on plasmid pCEFLGFP eIF5A at residue 47 and 50 Lysine (K) to Arginine (R). Mutation was introduced using the primers for eIF5AK47R_Fw (5′-gag atg tct act tcg agg act ggc aag cac ggc-3′), eIF5AK47R_Rv (5′-gcc gtg ctt gcc agt cct cga agt aga cat ctc-3′), eIF5AK50R_Fw'(5′-act tcg aag act ggc agg cac ggc cac gcc aag-3′) and eIF5AK50R_Rv'(5′-ctt ggc gtg gcc gtg cct gcc agt ctt cga agt'-3′) following the manufacturer's directions. Plasmids were sequenced by Eurofins (Louisville, KY, USA) to confirm mutations at K47/K50 residues.

2.4. Immunoprecipitation

Immunoprecipitation (IP) assay was performed as described elsewhere [25] with slight modifications. Briefly, LAP-wtTDP-43 cells were harvested and lysed in Co-IP Radioimmunoprecipitation assay buffer according to the manufacturer's descriptions (Pierce, MA, USA, # 20338). 10 μg protein was used as input while the remaining lysate was precleared at 4 °C with Protein A Trisacryl Resin beads (Pierce, MA, USA, # 20338) and conjugated to either TDP-43 (Proteintech, IL, USA, # 12892-1-AP) or isotype control IgG antibody (Thermo Fisher Scientific, MA, USA, # 31887). After antibody incubation, beads were rinsed 3 x with cold, sterile PBS, and resuspended in 50 μl of resuspension buffer (50 mM Tris HCl pH 7.4, 5 mM EDTA, 10 mM DTT, and 1% SDS) and denatured using 5 X SDS loading buffer. Input and IP samples were analyzed on a Western blot and probed with the following antibodies (Supplementary Table 4): $eIF5A^{Hyp\text{-}K50}$ (21st Century Biochemicals, MA, USA), TDP-43 (Sigma Aldrich, MO, USA, # WH0023435M1), and TIAIA-1 (Santa Cruz Biotechnology, TX, USA # sc-1751). The inputs were probed with either GAPDH (Proteintech, IL, USA, # HRP-60004) or β-Actin (Sigma Aldrich, MO, USA, A5441). IP was performed in triplicates and verified in four independent experimental set-ups.

2.5. Mass spectroscopy

M17 cells (ATCC, VA, USA, # CRL-2267) were harvested, and lysed with 1 X TBS. An IP was conducted as described in the manufacturer's user guide (Pierce™ NHS-Activated Magnetic Beads, MA, USA, # 88826). Beads were conjugated with the $eIF5A^{HypK50}$ antibody at a concentration of 0.5 μg of antibody/μg of beads. The hypusine-specific antibody, was manufactured by 21st Century Biochemicals, Inc., (Marlborough, MA, USA) and its specificity has been previously described [26]. 1.5 mg/mll of soluble protein from antibody-conjugated beads sample. Sample with no antibody was used as control. Protein extracts were separated by SDS-PAGE. Coomassie-stained gel pieces

were excised from the regions of interest. Briefly, gel pieces were minced and de-stained before being reduced with dithiothreitol (DTT), alkylated with iodoacetamide (IAA), and finally digested with Trypsin/Lys-C overnight at 37 °C. Peptides were extracted using 50/50 acetonitrile (ACN)/H_2O/0.1% formic acid and dried in a vacuum concentrator. Peptides were resuspended in 98%H2O/2%ACN/0.1% formic acid for LC-MS/MS analysis. Experiments were performed in triplicate in two independent experiments. Peptides were separated using a 75 μm × 50 cm C18 reversed-phase-HPLC column (Thermo Fisher Scientific, MA, USA) on an Ultimate3000 UPLC system (Thermo Fisher Scientific, MA, USA) with a 60-min gradient (4–40% ACN with 0.1% formic acid) and analyzed on a hybrid Quadrupole-Orbitrap instrument (Q Exactive Plus, Thermo Fisher Scientific, MA, USA). Orbitrap full MS survey scans were acquired at 60,000 resolution. The top 10 most abundant ions were selected for MS/MS analysis in the linear ion trap. Raw data files were processed in MaxQuant (www.maxquant.org) and searched against the most current UniprotKB human protein sequence database. Search parameters included constant modification of cysteine by carbamidomethylation and the variable modification, methionine oxidation. Proteins were identified using the filtering criteria of 1% protein and peptide false discovery rate. Proteins were ranked based on the number of unique peptides identified.

2.6. Gene ontology analysis

2.6.1. Ingenuity Pathway Analysis

Ingenuity Pathway Analysis (IPA) was used to illustrate both network interactions and enriched pathways associated with a data set of the top 50 proteins identified by mass spectrometry following co-immunoprecipitated with eIF5A^{HypK50}. The network used the IPA Connect tool within the MyPathways feature to display both direct and indirect protein interactions annotated across human, mouse, and rat species. Databases from Ingenuity third party sources were applied for curating the displayed interactions with confidence levels ranging from “experimentally observed” to “moderately predicted”. Nodes within the network are distinguished by both region and color to show the top four associated pathways identified by the IPA Metabolomics Core Analysis tool.

2.7. Enrichr analysis

Enrichr software was used for Gene Ontology (GO) analysis on the full data set of 887 proteins identified from the co-IP procedure with MS. Enrichr GO libraries are constructed from multiple biological and biomedical online databases to compare overlap of a queried dataset with annotated gene sets representative of functional attributes. The top 20 molecular functions and biological processes were ranked based on their relative combined scores; a comprehensive statistical parameter was used to associate annotated GO terms with the queried dataset.

2.8. Surface sensing of translation (SUnSET)

Changes in translation were evaluated with surface sensing of translation (SUnSET), which uses puromycin as a structural analog of aminoacyl tRNAs to prevent elongation after being incorporated into the nascent polypeptide chain. LAP-wtTDP-43 cells were grown on 6 well plates (n = 3) and treated with GC7 as described in the *Cell culture and treatment* section. After 72 h, cells were treated with 1 μM puromycin for 30 min at 37 °C, harvested and lysed with M-PER (Thermo Fisher Scientific, MA, USA, # 78501) containing protease inhibitor (Sigma Aldrich, MO, USA, # P8340), phosphatase inhibitor cocktails 2 and 3 purchased from Sigma Aldrich, MO, USA, # P5726, and # P0044 respectively, phenylmethylsulfonyl fluoride (0.1 M PMSF, Acros Organics, NJ, USA, # 215740050) and DNase (5 mg/mL, Alfa Aesar, MA, USA, # J62229) each at a 1:100 dilution. 20 μg of protein from each sample and standard was run on SDS-PAGE and Western blot. Standards were generated by mixing pooled puromycin-treated homogenates with pooled non-puromycin treated homogenates to desired percentages (100, 50, 25, 12.5, and 0% puromycin-treated). The membrane was probed puromycin (Millipore Sigma, MA, USA, # MABE343), eIF5A^{HypK50} (21st Century Biochemicals, MA, USA), and β-Actin (Abcam, Cambridge, UK, #ab13822).

2.9. Cellular fractionation and Western blot

LAP-wtTDP-43 were seeded on 15 cm cell culture dishes (n = 4), then treated as described in *Cell culture and treatment* section. Cells were washed and harvested with PBS and immediately followed by lysis with Sub-Cellular Fractionation Buffer (SFB) (250 mM sucrose, 10 mM KCl, 20 mM HEPES pH 7.4, 1.5 mM $MgCl_2$, 1 mM EDTA, and 1 mM EGTA) including protease inhibitor (Sigma Aldrich, MO, USA, # P8340), phosphatase inhibitor cocktail 2 and 3 purchased from Sigma Aldrich, MO, USA, # P5726, and # P0044 respectively, phenylmethylsulfonyl fluoride (0.1 M PMSF, Acros Organics, NJ, USA, # 215740050) and DNase (5 mg/mL, Alfa Aesar, MA, USA, # J62229) each at a 1:100 dilution. Samples were agitated at 4 °C for 10 min and then centrifuged at 14,000 RPM at 4 °C for 10 min. The resulting supernatant was collected as *cytoplasmic fraction*. The pellet was resuspended with SFB containing the inhibitors, agitated at 4 °C for 30 min followed by centrifugation at 14,000 RPM at 4 °C for 10 min. The resulting supernatant was collected as the *membrane fraction*. The remaining pellet was resuspended in RIPA buffer (50 mM Tris HCl, 150 mM NaCl, 2 mM EDTA, 0.1% SDS, 0.5% sodium deoxycholate, and 1% Triton x-100, pH 7.4), including the inhibitors, vortexed for 30 s, sonicated, and centrifuged at 14,000 RPM at 4 °C for 10 min. This fraction denotes cellular *nuclear proteins*. Pellets from each fraction were washed 3 x with PBS to ensure complete removal of prior proteins. 10 μg of protein was analyzed by Western blot and probed for the following antibodies (Supplementary Table 4): TDP-43 (Abnova, Taiwan, # H00023435-M01), eIF5A (Abcam, MA, USA, # ab32443), eIF5A$^{Hyp\text{-}K50}$ (21st Century Biochemicals, MA, USA, customized), Lamin A/C (Cell Signaling, MA, USA, 2032SeIF5A^{AcK47}(Assay Biotech, CA, USA, # D12065), GAPDH (Proteintech, IL, USA, # HRP-60004). Western blots were developed using Amersham imager 600 quick-start and analyzed using AlphaEaseFC software.

2.10. Soluble and insoluble protein isolation

LAP-wtTDP-43 cells were seeded in 6-well cell culture plates (n = 4) and treated similarly according to the *Cell culture and treatment* section then lysed for the soluble protein extraction using a RIPA buffer (50 mM Tris HCl, 150 mM NaCl, 2 mM EDTA, 0.1% SDS, 0.5% sodium deoxycholate, and 1% Triton x-100, pH 7.4) including the protease and phosphatase cocktail 2 and 3 inhibitors (Sigma Aldrich, MO, USA, # P5726, and # P0044 respectively), PMSF (Acros Organics, NJ, USA, # 215740050), and DNase (Alfa Aesar, MA, USA, # J62229) each at a 1:100 dilution. Samples were centrifuged at 14,000 RPM at 4 °C for 10 min and the supernatant was stored as the RIPA soluble fraction. Pellet was rinsed in RIPA buffer, briefly centrifuged and the resulting pellet was then resuspended in urea buffer (7 M urea, 2 M Thiourea, 4% CHAPS, and 30 mM Tris, pH 8.5), sonicated, and centrifuged at 100,000 × *g* at 4 °C for 30 min. The supernatant was collected and used as the urea soluble fraction. Immunoblot analysis was performed using 5 μg of protein and probed with the following antibodies: TDP-43 (EMD Millipore, MA, USA, # MABN150), phospho TDP-43 (pS409/410-2) (Cosmo Bio Co, CA, USA, # TIP-PTD-P02), β-Actin (Sigma-Aldrich, MO, USA, # A5-441).

2.11. Immunocytochemistry and confocal imaging

LAP-wtTDP-43 cells were initially seeded for 24 h on fibronectin (2 μg/mlll, Sigma Aldrich, MO, USA, #F2006) coated coverslips

(Fisherbrand, PA, USA, # 22031145) and treated as described in the *Cell culture and treatment* section. Cells were fixed with 4% paraformaldehyde then permeabilized and blocked with 0.2% Triton x-100 and 3% HI-FBS in PBS for 1 h. Cells were immunostained for 2 h using the following antibodies (Supplementary Table 4): TIAAI-1 (Santa Cruz Biotechnology, CA, USA, # sc-1751), TDP-43 (Abnova, CA, USA, # H00023435-M01), eIF5A (Abcam, MA, USA, # ab32443) and eIF5A^{HypK50} (21st Century Biochemicals, MA, USA, customized). Cells were incubated for 45 min at room temperature with corresponding Alexa Fluor secondary antibodies (Invitrogen, CA, USA). Slides were coverslipped with Vectashield Hardset Mounting Medium with DAPI (Vector Laboratories, CA, USA, # H1500) or Prolong Gold Antifade Mountant (Thermo Fisher Scientific, MA, USA, # P36934). In some instances, nuclei were stained using Hoechst 33342 (Thermo Fisher Scientific, MA, USA, # H3570).

Images were obtained with an LSM880 Carl Zeiss Confocal Microscope using immersion oil with a 63× lens objective. Images for each fluorophore were obtained by sequential scanning where at least ten fields of interest were obtained with an average z-stack of eight frames per field. Images were merged and recovered using the ZEN microscope software. Co-localization analyses were carried out using Image J, and thresholding was kept constant across all pictures. *Z*-stack images taken for immunocytochemistry were acquired utilizing the Olympus Fluoview fv10i on the 63× water objective. Images were merged with Fv10i software.

2.12. Statistical analysis

Statistical analyses were performed using Student's *t*-test or one-way ANOVA followed by Tukey *post-hoc* means comparison test. The Western Blot analysis protein was normalized to GAPDH or actin expression. Values are represented as the standard error of the mean (SEM). P values were considered statistically significant when compared to untreated control as followed: *$p < 0.05$, **$p < 0.01$ and ***$p < 0.001$. Statistical significance, when compared to SA treated sample, is denoted as #; $p < 0.05$. Graphs were generated using GraphPad Prism 8.4 software (GraphPad Software, CA, USA).

3. Results

3.1. Protein-protein interactions of hypusinated eIF5A identified networks associated with neurodegenerative disorders

Considering the regulatory role of eIF5A^{HypK50} in the translation of factors involved in stress response as well as SG assembly [27] and the emerging effect of TDP-43 accumulation in the cytoplasm and SGs [10,11,27–29] led us to explore the converging pathways between hypusinated eIF5A (eIF5A^{HypK50}) and TDP-43 in relevant cellular models. We performed IP in human neuroblastoma M17 cells using an antibody against eIF5A^{HypK50} (21st Century Biochemicals, MA, USA). Mass spectrometry analysis identified a total of 886 proteins (data submitted to ProteomeExchange). Proteins were sorted by the intensity and unique peptides, and the top 50 proteins were used for bioinformatic analysis using IPA. Analysis of the top 50 proteins identified three pathways that many of the identified proteins are involved in (network shown in Fig. 1A): RNA Post-Transcriptional Modification/RNA Damage and Repair/Molecular Transport (light pink); Cellular Function and Maintenance/Molecular Transport/Cell Signaling Interactions (light blue) and Cell Death and Survival/Cellular Function and Maintenance (yellow). Additionally, IPA identified a significant representation of nuclear transport proteins that co-immunoprecipitated with eIF5A^{HypK50} (highlighted). The full list of functional associations of these pathways, based on IPA scoring parameters, is shown in Supplementary Table 1.

Importantly within the proteome, the association between eIF5A^{HypK50} and TDP-43 was amongst the top seventh interactions identified in these cells, supporting the notion of a possible biological relevance between both proteins. Interestingly, several proteins associated with neurological disorders were found amongst the eIF5A^{HypK50} interactome. For example, we identified the microtubule-associated

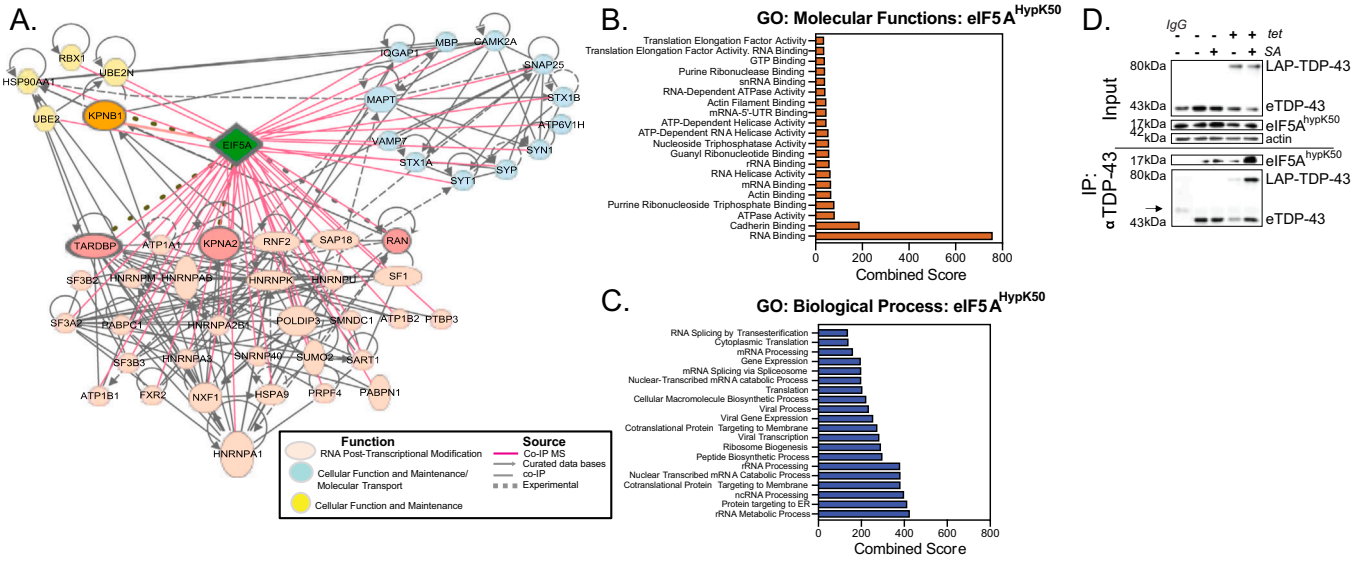

Fig. 1. The IPA and functional analysis identified protein networks interacting with hypusinated eIF5A. A. Ingenuity Pathway Analysis was used to determine the canonical pathways associated with the 50 most abundant proteins enriched in the eIF5A^{HypK50} immunoprecipitation. The proteins are clustered based on the top 3 associated canonical pathways; RNA Post-Transcriptional Modification, RNA Damage and Repair, and Molecular Transport (light pink); Cellular Function and Maintenance, Molecular Transport, and Cell Signaling Interactions (light blue); Cardiovascular Disease, Cell Death and Survival, Cellular Function and Maintenance (yellow). Full red and black lines represent the predicted relationship between proteins as identified by mass spectrometry analysis and curated IPA. Dashed and dotted lines represent experimentally observed relationships. Proteins examined in this study were bolded. B, C. The top 20 molecular functions and biological processes associated with all proteins identified by proteomics. The entire dataset (886 proteins) was analyzed using Enrichr software with the GO: database, and the top 20 most significant ($p < 0.05$, combined scored) molecular functions and biological processes are shown. D. LAP-wtTDP-43 cells (+/- tetracycline, tet) and treated with 0.5 mM SA were immunoprecipitated with anti-TDP-43 or isotype IgG control antibodies; both IP and input lysate samples were probed with antibodies against TDP-43 and eIF5A^{HypK50}. Arrow denotes the IgG band.

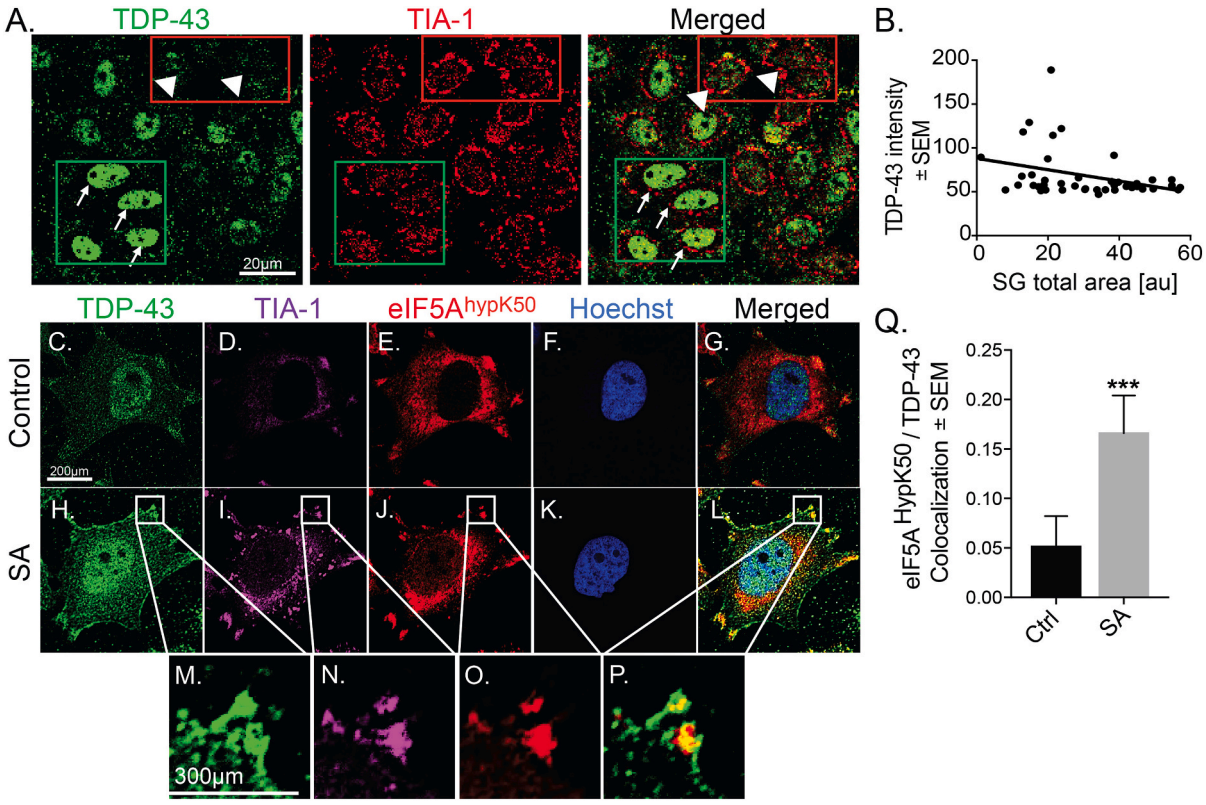

Fig. 2. Hypusinated eIF5A co-localizes with accumulated TDP-43 in stress granules during SA-induced cellular stress. A. Immunofluorescence images of wtTDP-43 cells treated with 0.5 mM SA and stained for TDP- 43 (green), TIA-1 (red) and merged. B. Scatter plot representation of Image J analysis demonstrating the correlation between TDP-43 intensity and stress granule total area in the cytoplasm based on TIA-1 signal. Linear regression, $r^2 = 0.09$, slope = − 0.64 (± 0.28), *p < 0.05, n = 41 cells/experiment. C–P. Immunofluorescence images of wtTDP-43 cells immunofluorescence stained for TDP-43 (green), TIA-1 (purple), eIF5A^{HypK50} (red), Hoechst 33342 (blue), and the merged image. C–G. Untreated cells, H–L. Cells treated with 0.05 mM SA for 1 h and M–P. magnified images of TDP-43 positive stress granules in SA-induced cells. Q. Co-localization between eIF5A^{HypK50} and TDP-43 in the cytoplasmic TIA-1 positive granules, MOC analysis, n = 10 cells/condition/experiment. Student *t*-test, ***p < 0.001.

protein tau (MAPT), implicated in the neuropathology of various tauopathies and Alzheimer's disease [30], was associated with eIF5A^{HypK50}. Other potential partners of eIF5A^{HypK50} included; syntaxin (STX1A), the determining factor for intelligence level in Williams Syndrome patients [31], Myelin basic protein (MBP), involved in demyelinating diseases such as multiple sclerosis [32], Synaptosomal associated Protein 25 kDa (SNAP-25) and Vesicle associated membrane proteins (VAMP), both associated with neurological disorders such as schizophrenia, attention-deficit/hyperactivity disorder and epilepsy [33].

Next, we employed Enrichr and Gene Ontology (GO) functional enrichment analysis on the full 886-protein interactome to annotate the biological relevance of the identified interactions (Fig. 1B, C). Not surprisingly, the "RNA-binding" and "rRNA Processing" were the most represented molecular functions and biological processes enriched within our data set. Computational ranking by the combined score indicated RNA-binding to be 3.75–5-fold higher than all other molecular functions as identified by GO analysis (Fig. 1B, Supplemental Table 2). Also, SRP-dependent co-translational protein targeting to membrane, ncRNA processing, protein targeting to ER, and rRNA metabolic processes were between 1.3 and 2-fold higher compared to the other categories within the biological processes recognized (Fig. 1C, Supplemental Table 3).

Considering our proteomics findings and the suggested functional interaction between eIF5A^{HypK50} and TDP-43 observed in Ba/F3 cell line [23], we aimed to investigate the biological function of such interaction in further detail. We utilized wild type TDP-43 overexpressing tetracycline-regulatable isogenic HeLa cells (LAP-wtTDP-43 cells), (Fig. 1D). Sodium arsenite (SA) is used by many studies as a cellular stressor to achieve TDP-43 cytoplasmic localization and accumulation to SGs [10,34]. Therefore, cells were treated with 1 μg/ml tetracycline for 24 h, followed by 0.5 mM SA for 1 h, before IP using an antibody against human TDP-43 (Fig. 1D). Both input and IP fractions were analyzed by Western blot. The input fraction showed expression of both LAP-wtTDP-43 (80 kDa band) and endogenous wtTDP-43 (43 kDa band) upon tetracycline treatment (tet+), while only endogenous wtTDP-43 is present in the untreated cells (tet-, Fig. 1D). Conversely, eIF5A^{HypK50} was present in all cellular samples and was slightly increased followed SA treatment. Interestingly, the IP fraction demonstrated co-precipitation of both endogenous TDP-43 and LAP-TDP-43 with eIF5A^{HypK50}. Increased eIF5A^{HypK50} band intensity was observed in tet+/SA treated cells. The IgG isotype control did not yield any of the protein bands except the IgG band (arrow). Overall, the co-IP results confirmed the proteomics findings and suggested that the association between TDP-43 with eIF5A^{HypK50} might strengthen with stress and TDP-43 overexpression in this cellular model.

3.2. eIF5A^{HypK50} colocalizes with TDP-43 in stress granules during arsenite-induced stress

Data suggesting regulation of TDP-43 in the SG [35] prompted us to further investigate the role of eIF5A^{HypK50} in TDP-43 accumulation during stress. Cells treated as described above underwent immunocytochemical assay and were labeled against TDP-43 and T-Cell-Restricted Intracellular Antigen-1 (TIA-1), an RNA binding protein and SG marker shown to co-localize with TDP-43 [10,34]. Confocal imaging demonstrated TDP-43 integration into the SGs (Fig. 2A). Moreover, our analysis indicated that the accumulation of TDP-43 altered SG

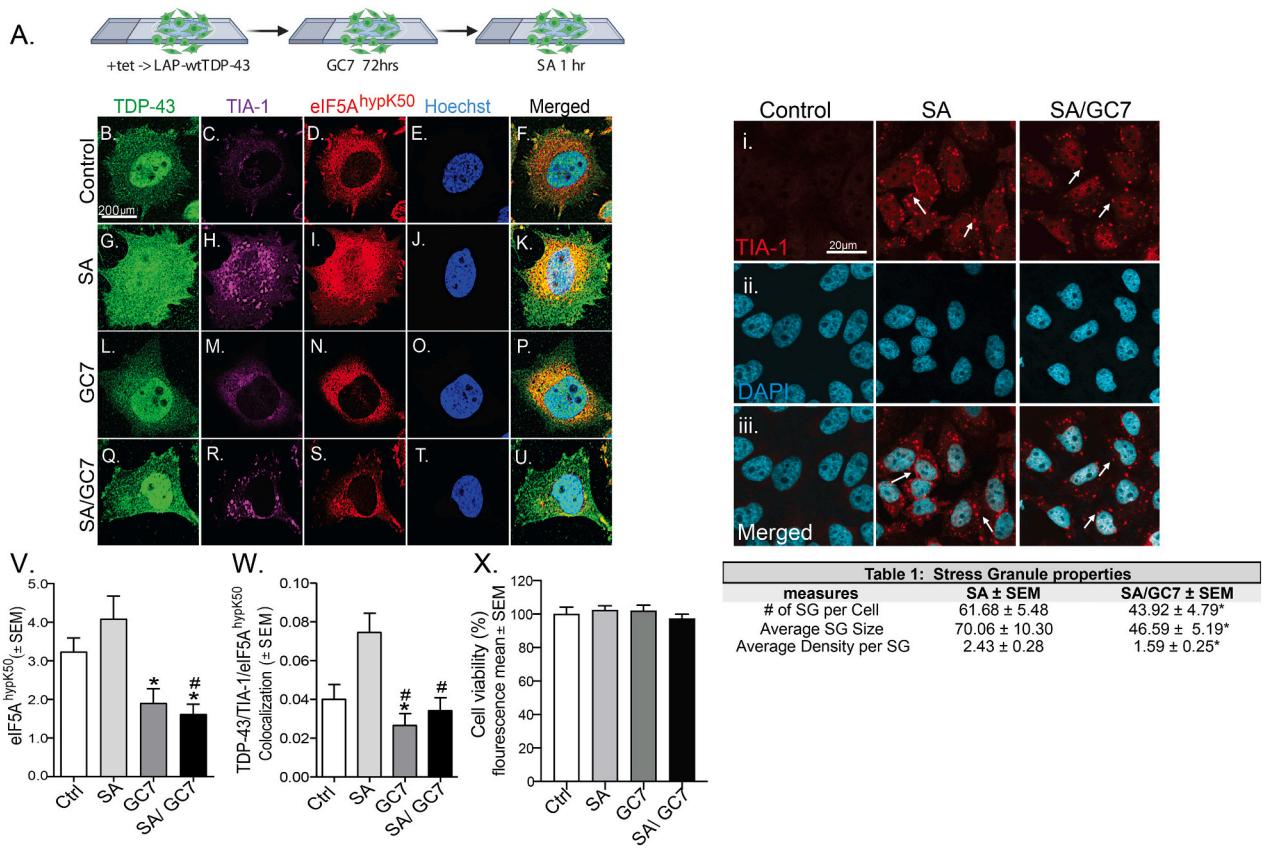

Table 1: Stress Granule properties		
measures	SA ± SEM	SA/GC7 ± SEM
# of SG per Cell	61.68 ± 5.48	43.92 ± 4.79*
Average SG Size	70.06 ± 10.30	46.59 ± 5.19*
Average Density per SG	2.43 ± 0.28	1.59 ± 0.25*

Fig. 3. Reduction of hypusination decreased TDP-43 accumulation and co-localization with eIF5A^{HypK50} during cellular stress. A. HeLa treatment paradigm flow-chart. B–U. Immunolabeled image of LAP wtTDP-43 (tet +) cells stained for TDP-43 (green), TIA-1 (purple), eIF5A^{HypK50} (red), Hoechst 33342 (blue), and the merged images. B–F. Untreated and G–K. treated cells with 0.5 mM SA, L.–P. or 30 μM GC7, and Q.–U. 30 μM GC7 followed by 0.5 mM SA. V. Levels of eIF5A^{HypK50} in the cell was determined by ImageJ analysis. W. Co-localization of TDP-43 with eIF5A^{HypK50} in TIA-1 positive regions in the cytoplasm was determined by MOC analysis. X. Cellular viability in treated HeLa cells was determined by the fluorescence intensity of AlamarBlue assay. Statistical analysis was performed by one-way ANOVA followed by Tukey post-hoc test (n = 10 cells/condition, each experiment was repeated three times), * $p < 0.05$. # denotes statistical significance ($p < 0.05$) compared to the SA treated sample. Immunolabeled images of tet-induced LAP wtTDP-43 cells following SA-induced stress and stained for i. TIA-1 (red), ii. DAPI (blue), and the iii. merged image. n = 82–98 cells/treatment *$p < 0.05$.

Table 1
Stress granule properties.

Measures	SA ± SEM	SA/GC7 ± SEM
# of SG per cell	61.68 ± 5.48	43.92 ± 4.79*
Average SG size	70.06 ± 10.30	46.59 ± 5.19*
Average SG density	2.43 ± 0.28	1.59 ± 0.25*

P values were considered statistically significant compared to SA group as followed: *$p < 0.05$. Student t-test

characteristics and high TIA-1 signal, and large SG size corresponded to cells with a low TDP-43 signal. In contrast, cells with high TDP-43 signal intensity exhibited low TIA-1 signal intensity and smaller SG size (Fig. 2B, $p = 0.03$). The significant inverse correlation between the nuclear TDP-43 signal and the total area of TIA-1 positive SG are shown in Fig. 2B.

The notion that TDP-43 and eIF5A^{HypK50} may interact physiologically and accumulate in SG led us to investigate the spatial relationship of TDP-43 and eIF5A^{HypK50} in SG and during SA-induced stress. LAP-wtTDP-43 cells were treated as before and immunolabeled with antibodies against TDP-43, eIF5A^{HypK50}, and TIA-1 (Fig. 2C-P). As expected, treatment with SA induced the formation of TIA-1 positive SGs (I and N) resulting in the mislocalization of TDP-43 into the cytoplasm and accumulation into SG (C, H, and M). Interestingly, stress prompted hypusination of cytoplasmic eIF5A (E and J). We also observed increased co-localization of TDP-43 and eIF5A^{HypK50} in TIA-1 positive SGs during stress (M-P), which was further confirmed by Manders overlaping coefficient (MOC) analysis (Fig. 2Q, ***$p < 0.001$).

3.3. Reduction of hypusination prevents eIF5A binding with TDP-43 in stress granules

Induced TDP43-eIF5A^{HypK50} co-localization in SGs during stress and the canonical role of eIF5A in SG assembly led us to hypothesize that eIF5A regulates accumulation of TDP-43 in SGs in a hypusine-dependent manner. To explore this plausible pathway, we utilized the deoxyhypusine synthase inhibitor, N1-guanyl-1, 7-diaminoheptane (GC7, IC_{50}, 17 nM) [20], as it was previously reported to significantly reduce hypusination and SG assembly [27]. LAP-wtTDP-43 cells treated with 30 μM GC7 for 72 h and followed by treatment with 0.5 mM SA for 1 h. Cells were stained against TDP-43, eIF5A^{HypK50} and TIA-1 (Fig. 3A, B-U). Per our previous findings, SA induced TDP-43 mislocalization to the cytoplasm and in TIA-1 positive SGs (Fig. 3G, H). Additionally, immunocytochemistry images showed that GC7 treatment reduced hypusination levels in cells (Fig. 3N, S). Image J stain intensity analysis revealed that GC7 significantly decreased hypusination in both SA-treated and untreated cells (Fig. 3V, *$p < 0.05$, $^{\#}p < 0.05$ compared to the SA treated sample). Similarly, MOC analysis determined significant co-localization between TDP-43 and eIF5A^{HypK50} in SGs, which was reduced following GC7 treatment (Fig. 3W, *$p < 0.05$, $^{\#}p < 0.05$ compared to the SA treated sample). Additionally, we demonstrated that neither SA nor GC7 treatment reduced the cellular viability of LAP-

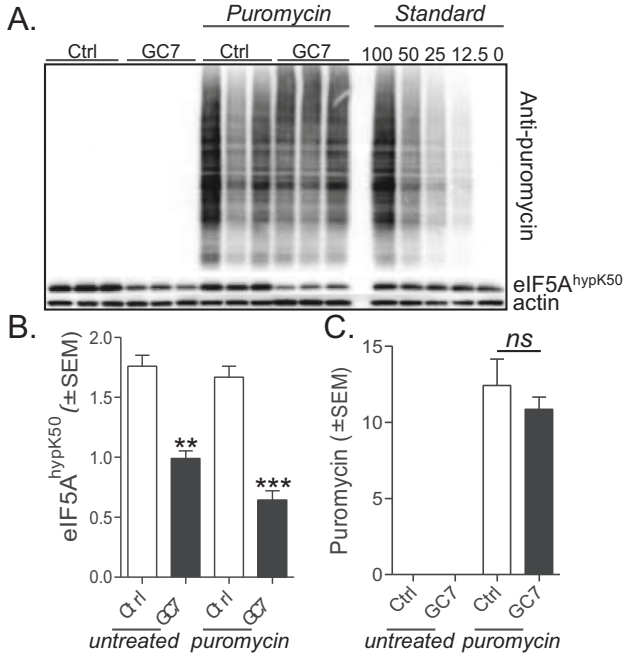

Fig. 4. Nascent protein synthesis is not impaired following a reduction in hypusination levels. SUnSET assay measuring puromycin incorporation into proteins during translation in LAP wtTDP-43 (tet +) cells treated with 30 μM GC7. A. Western blot of puromycin-tagged proteins, cellular standards, and eIF5AHypK50 levels are shown. B. Quantification of hypusine levels in cells following puromycin treatment. C. Levels of puromycin incorporation during protein synthesis. Cellular extracts with known protein amounts were used as standards for quantification purposes (100, 50, 25, 12.5, and 0% puromycin-treated). Actin is used as a loading control. Statistical analysis was performed by one-way ANOVA followed by Tukey post-hoc test. ** $p < 0.01$, *** $p < 0.001$, *ns.* not significant.

wtTDP-43 HeLa cells, as measured by Alamar Blue cell viability assay (Fig. 3X).

Next, we analyzed the impact of GC7 treatment on SG characteristics, as identified by the positivity for TIA-1 expression (Fig. 3i-iii). The number of SGs, size, and density was analyzed (n = 82–98 cells per treatment). Indeed, cells treated with GC7/SA significantly decreased the number of SGs, the average granule size, and density in comparison to SA treated cells (Table 1, *$p < 0.05$).

3.4. Reduction of eIF5A hypusination does not affect global protein synthesis

Although eIF5A is intimately involved in eukaryotic cell proliferation, the true physiological function of eIF5A has yet to be elucidated. For example, studies in *S. cerevisiae* mutant strain observed that the depletion of eIF5A generated only a relatively small inhibition of protein synthesis [36], while the polysome profiles of *S. cerevisiae* temperature-sensitive mutants provided evidence that eIF5A distinctly effects translation elongation [17]. To investigate whether the observed changes in TDP-43 levels are a direct or indirect consequence of reduced "de novo" protein synthesis, we performed surface sensing of translation (SUnSET) assay as previously published [37]. In this assay, treatment with puromycin is incorporated into the nascent protein, hence allowing oversight onto the protein synthesis levels. Tet-induced LAP-wtTDP-43 cells were treated with 30 μM GC7 for 72 h, then with 1 μM puromycin for 30 min at 37 °C. Immunoblot assay was performed and probed with antibodies against puromycin and eIF5A^{HypK50} (Fig. 4A). Puromycin incorporation was standardized against standard samples. As expected, GC7 treatment significantly reduced levels of hypusination in treated cells (Fig. 4B, **$p < 0.01$, ***$p < 0.001$). However, GC7 treatment did not alter puromycin levels compared to standards and controls (Fig. 4C). We, therefore, determined that reduction in hypusine levels via GC7 did not affect overall protein synthesis in this cellular model.

3.5. Decreased cytoplasmic TDP-43 levels following reduction of eIF5A^{HypK50}

Next, we aimed to investigate the effects of reduced hypusination on the cytoplasmic localization of TDP-43. Following our experimental paradigm, cells were fractionated in cytoplasmic and nuclear protein pool and analyzed by immunoblot (Fig. 5A). Treatment with GC7 significantly reduced eIF5A^{HypK50}, while inversely increasing levels of eIF5A^{AcK47} in the cytoplasmic fraction (Fig. 5B, *$p < 0.05$, **$p < 0.01$, ***$p < 0.001$, $^{\#}p < 0.05$ compared to the SA treated sample). As acetylation of K47 within the "hypusine loop" represents another post-translational modification of eIF5A and competes with the ability to convert K50 to hypusine [38], our data confirm the inverse relationship of both post- translational modifications.

Importantly, cytoplasmic to the nuclear ratio of LAP-TDP-43 and endogenous TDP-43 (eTDP-43) revealed a significant increase of TDP-43 levels in the cytoplasm of SA treated cells compared to the control sample (Fig. 5C, *$p < 0.05$, ***$p < 0.001$). Cells treated with GC7 alone demonstrated a slight reduction in TDP-43 cytoplasmic levels, however, stressed cells treated with GC7 significantly reduced cytoplasmic TDP-43 accumulation. We further found that this was followed by induced nuclear levels of both LAP- and endogenous TDP-43 (Fig. 5C, $^{\#}p < 0.05$ compared to the SA treated sample). These findings suggest that reduction in hypusine levels regulates cytoplasmic TDP-43 accumulation by possibly rescuing the nuclear re-entry of TDP-43.

3.6. Hypusine dependent interactions of eIF5A with nuclear transport machinery proteins

To further investigate the nucleocytoplasmic shuttling of TDP-43 we returned to the mass spectrometry data and protein cluster analysis. Interestingly, within the IPA analysis, we identified a cluster of nuclear transport proteins that co-IP with eIF5A^{HypK50}; that included KPNA1 (importin subunit α5), KPNA2 (importin subunit α1), KPNB1 (importin subunit β), and RanGTP (Fig. 6A). These proteins are part of the nuclear importin complex responsible for binding to cytoplasmic cargo via nuclear localization signals (NLS) and translocation through the nuclear pore complex (NPC) [39,40]. RanGTP is essential for the nuclear transport of cargo protein via the NPC into the nuclear interior [41–43]. To determine whether modifications of the hypusine levels affect nuclear transport machinery, we investigated importin's cytoplasmic localization and expression by immunoblot assay (Fig. 6B). Analysis of the cytoplasmic fraction indicated that stress alone was insufficient to modify the cytoplasmic levels of the NPC proteins. However, GC7 treatment in SA-stressed cells significantly reduced KPNA1, KPNB1, RanGTP levels (Fig. 6C, *$p < 0.05$) but not KPNA2 ($p = 0.07$). Altogether, our data demonstrate that reduced hypusination alters cytoplasmic importin levels and possibly facilitated their nuclear gradient.

3.7. Reduced eIF5A hypusination decreases insoluble TDP-43 levels following cellular stress

A hallmark of pathology is the cytoplasmic presence of hyperphosphorylated and aggregated TDP-43 [44]. To determine whether hypusination affected TDP-43 phosphorylation and aggregation, we isolated RIPA and Urea-soluble cellular fractions of treated tet-induced LAP-wtTDP-43 cells (Fig. 7A). Immunoblots from each fraction were probed with antibodies against total and phosphorylated TDP-43 at serine 409/410 epitope (pTDP-43, Fig. 7B). We observed an immediate and significant increase in insoluble LAP-TDP-43 and endogenous TDP-

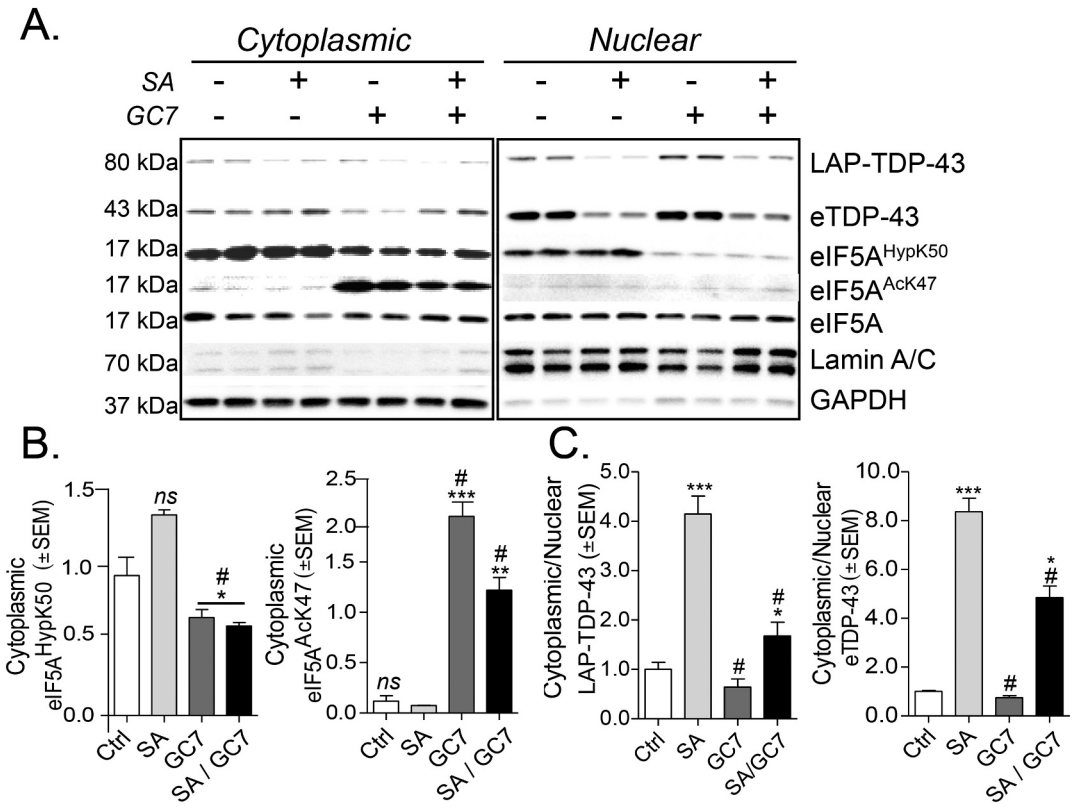

Fig. 5. Reduction of hypusination prevents cytoplasmic mislocalization of TDP-43. A. Immunoblot of the subcellular fractions of LAP wtTDP-43 cells following treatment. The cytoplasmic and nuclear fractions were probed for endogenous TDP-43, LAP-TDP-43, hypusinated and acetylated eIF5A. B. Densitometry quantification of cytoplasmic $eIF5A^{HypK50}$ and $eIF5A^{AcK47}$ levels normalized to actin. C. Cytoplasmic to the nuclear ratio of endogenous and LAP-TDP-43 levels following treatment. Statistical analysis was determined by one-way ANOVA followed by Tukey post-hoc test; *p < 0.05, **p < 0.01, ***p < 0.001, or *ns.* not significant, # p < 0.05, when compared to SA treated sample.

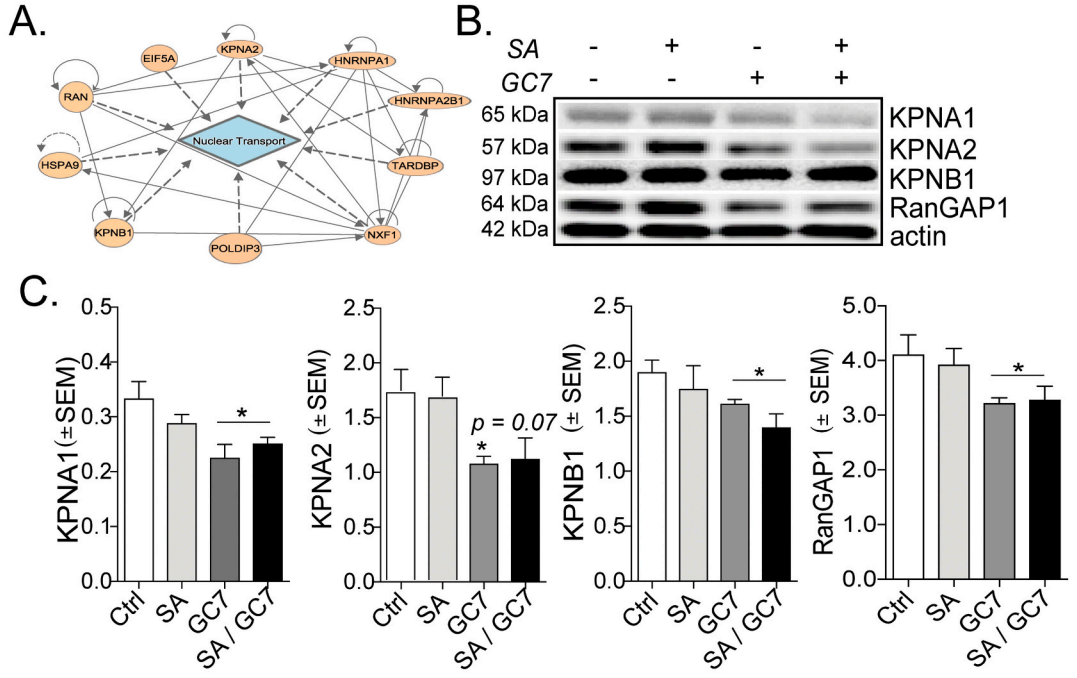

Fig. 6. A. Mass spectrometry and IPA analysis identified a cluster of nuclear transport proteins interacting with $eIF5A^{HypK50}$. B. Immunoblot of the cytoplasmic levels for RAN, KPNA1, and 2 and KPNB1 proteins. C. Densitometry quantification of cytoplasmic levels of RAN, KPNA1, and 2 and KPNB1 normalized to actin. Lamin A/C, GAPDH, or actin were used as loading controls. Statistical analysis was determined by one-way ANOVA followed by Tukey post-hoc test; *p < 0.05.

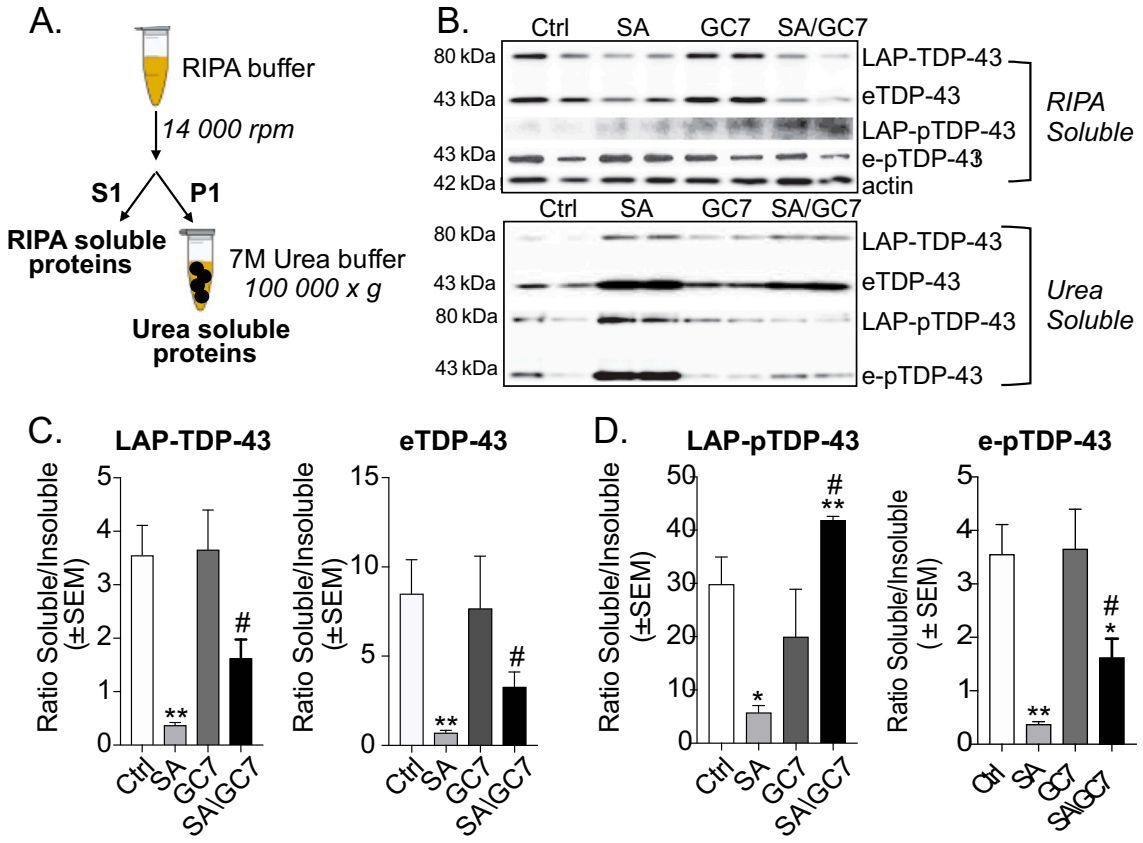

Fig. 7. -Reduced eIF5A hypusination decreases insoluble TDP-43 levels following cellular stress. A. Description of the RIPA and Urea fractionation method used to separate soluble and insoluble proteins from treated LAPwtTDP-43 (tet+) cells. B. Western blot determined total and phosphorylated Ser409/410 TDP-43 levels in RIPA and Urea-treated fractions. C. Densitometry quantifications of soluble to insoluble protein ratio. Actin was used as a loading control for the RIPA soluble fraction. Statistical analysis was determined by one-way ANOVA followed by Tukey post-hoc test, # denotes statistical significance ($p < 0.05$) compared to the SA treated sample, *$p < 0.05$, **$p < 0.01$, # denotes comparisons to the SA treated sample.

43 (eTDP-43) after 1 h of SA treatment compared to the untreated sample (Fig. 7C). GC7 alone did not affect the solubility of the protein compared to the untreated sample. However, stressed cells treated with GC7 significantly reduced insoluble TDP-43 and recovered the levels of soluble LAP-TDP-43 and eTDP-43 levels compared to SA treated cells ($p < 0.05$, # compared to SA).

Next, we analyzed levels of phosphorylated S409/410 TDP-43 and revealed that stress significantly induced phosphorylation and insolubility of both LAP-pTDP-43 and e-pTDP-43 when compared to the untreated cells (Fig. 7D, *$p < 0.05$ and **$p < 0.01$, respectively). GC7-treated cells only slightly reduced insoluble LAP-pTDP-43 levels. Importantly, following SA stress, GC7 treatment significantly reduced the insoluble pTDP-43 levels and recovered the soluble LAP-pTDP-43 and e-pTDP-43 protein levels (**$p < 0.01$, compared to the untreated sample, $p < 0.05$, # compared to SA).

These findings together provide first-time evidence for a direct role of eIF5A^{HypK50} in TDP-43 biology, where pharmacological reduction of hypusination reduces phosphorylated and insoluble TDP-43 levels.

3.8. Site-directed mutagenesis of the hypusine loop regulates TDP-43 phosphorylation levels

To further investigate the role of the hypusine loop modifications in TDP-43 pathology, we performed site-directed mutagenesis. The pCEFL-GFP eIF5A plasmid backbone was modified from lysine to arginine at lysine 47 and 50 of the hypusine loop (GFP-eIF5A^{K50R} and GFP-eIF5A^{K47R}, Fig. 8A). Both plasmids were overexpressed in the human Hek293T cell line. Untreated cells and cells transfected with non-mutated eIF5A plasmid (GFP-eIF5A) were included as controls. Cells were also co-transfected with two additional plasmids, DHS and DOHH (Flag-DOHH/DHS), as it has been suggested that DHS and DOHH activity is needed for the hypusination of exogenous eIF5A [45]. As expected, eIF5A protein did not undergo hypusination or acetylation in cells transfected with GFP-eIF5A^{K50R} and GFP-eIF5A^{K47R}, respectively (lane 7 & 8 vs. lane 9 & 10) (Fig. 8B). We also found that co-expression of eIF5A with DHS/DOHH was not required for exogenous or endogenous eIF5A hypusination (lanes 3 & 4 vs. 5 & 6) as similar hypusination levels were maintained following each condition (Fig. 8C). In addition, eIF5A alone or in co-expression with DHS/DOHH significantly induced total TDP-43 levels, while mutations did not significantly affect such levels (Fig. 8B and D). However, the expression of GFP-eIF5A^{K50R} (loss of hypusination) led to dramatic reductions in levels of phosphorylated S409/410 TDP-43 compared to cells expressing induced hypusination constructs (lanes 3–8) and untreated cells (lane 1 & 2, Fig. 8B and D). Conversely, pS409/410 TDP-43 levels were significantly increased in cells transfected with either GFP-eIF5A, GFP-eIF5A/Flag-DHS/DOHH or GFP-eIF5A^{K47R} (loss of acetylation, Fig. 8D). We found no changes in the expression levels of endogenous total and hypusinated eIF5A (Fig. 8B, C). Taken together, our data provide mechanistic evidence on the role of acetylation vs. hypusination in cytoplasmic accumulation of TDP-43. The dynamics of both acetylation and hypusination within the eIF5A hypusine loop might provide a novel entry-point for future therapeutic targets in TDP-43 proteinopathies.

4. Discussion

This study demonstrates a key role of hypusinated eIF5A in TDP-43 pathology in an SA-induced stress cellular model. We found that

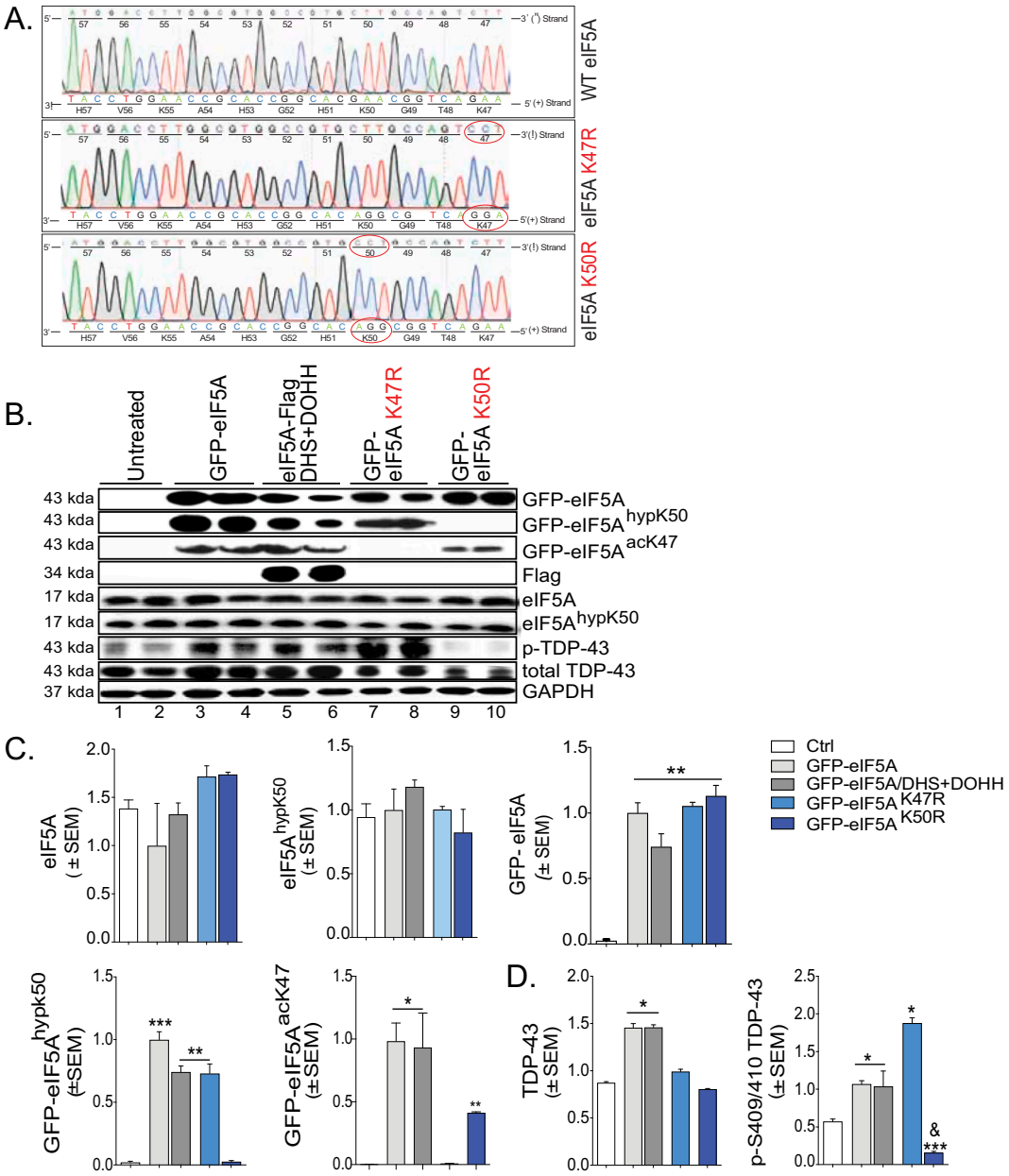

Fig. 8. Site-directed mutagenesis of eIF5A at lysine (K)50 and K47 modulate the phosphorylation of TDP-43. A. Site-directed mutagenesis of wild type GFP-eIF5A yield the substitution mutants at K47R and K50R (red circles). The chromatogram was obtained by sequencing the antisense strand of pCEFLGFP-eIF5A plasmid using primer sp6. Corresponding mutated sequences are highlighted with the red circle. B. Hek293T cell transfection was performed as described and the cytoplasmic fraction was analyzed by Western blot with antibodies against eIF5A^{HypK50} and eIF5A^{AcK47}, total eIF5A, Flag, total TDP-43, and pS409/410 TDP-43. C, D. Densitometry quantifications of cytoplasmic levels of each protein. GAPDH was used as a loading control. Statistical analysis was performed by one-way ANOVA with Tukey post-hoc test. *p < 0.05, **p < 0.01 ***p < 0.001.

reduction of hypusination alleviates TDP-43 cytoplasmic mislocalization and the accumulation into SGs. Our proteomics and functional data demonstrated a physiological interaction between eIF5A^{HypK50} and TDP-43, which was exacerbated during induced cellular stress and TDP-43 overexpression. We also report that reduction of hypusination by GC7 or mutagenesis led to decreased cytoplasmic total TDP-43 levels, phosphorylated and insoluble TDP-43 in two separate cellular models. Interestingly, we show that GC7 significantly reduced co-localization between TDP-43 and eIF5A^{HypK50} both in the cytoplasm and SGs following SA-induced cellular stress. Importantly, we observed that reduced hypusine levels neither affected the general "de novo" protein synthesis nor cellular growth of HeLa cells. In agreement with our findings, others have shown that HeLa cells treated with eIF5A-shRNA displayed a growth curve similar to that of the non-transduced cells up to 72 h. Measurements of total protein synthesis by pulse labeling with [3H]leucine revealed relatively small inhibition (< 20%) and authors concluded there is no global inhibition of protein synthesis when eIF5A is depleted [36].

Using mass spectrometry and protein interactome analysis, we identified key associated functional networks between eIF5A^{HypK50} and proteins within the "RNA-binding" and "rRNA Processing" biological and molecular processes. Interestingly, TDP-43 protein was one of the RNA-binding proteins (RBPs) that was highly scored in our data-set and implicated in the neuropathology of the ALS-FTD-AD spectrum of dementias [4,44,46]. Several studies have demonstrated that top RBPs, such as TDP-43, TIA-1, and FUS, harbor a canonical RNA recognition motif (RRM) and low-complexity domains critical for the formation of pathological aggregates in cytoplasm and SGs in brain. [47–49]. These

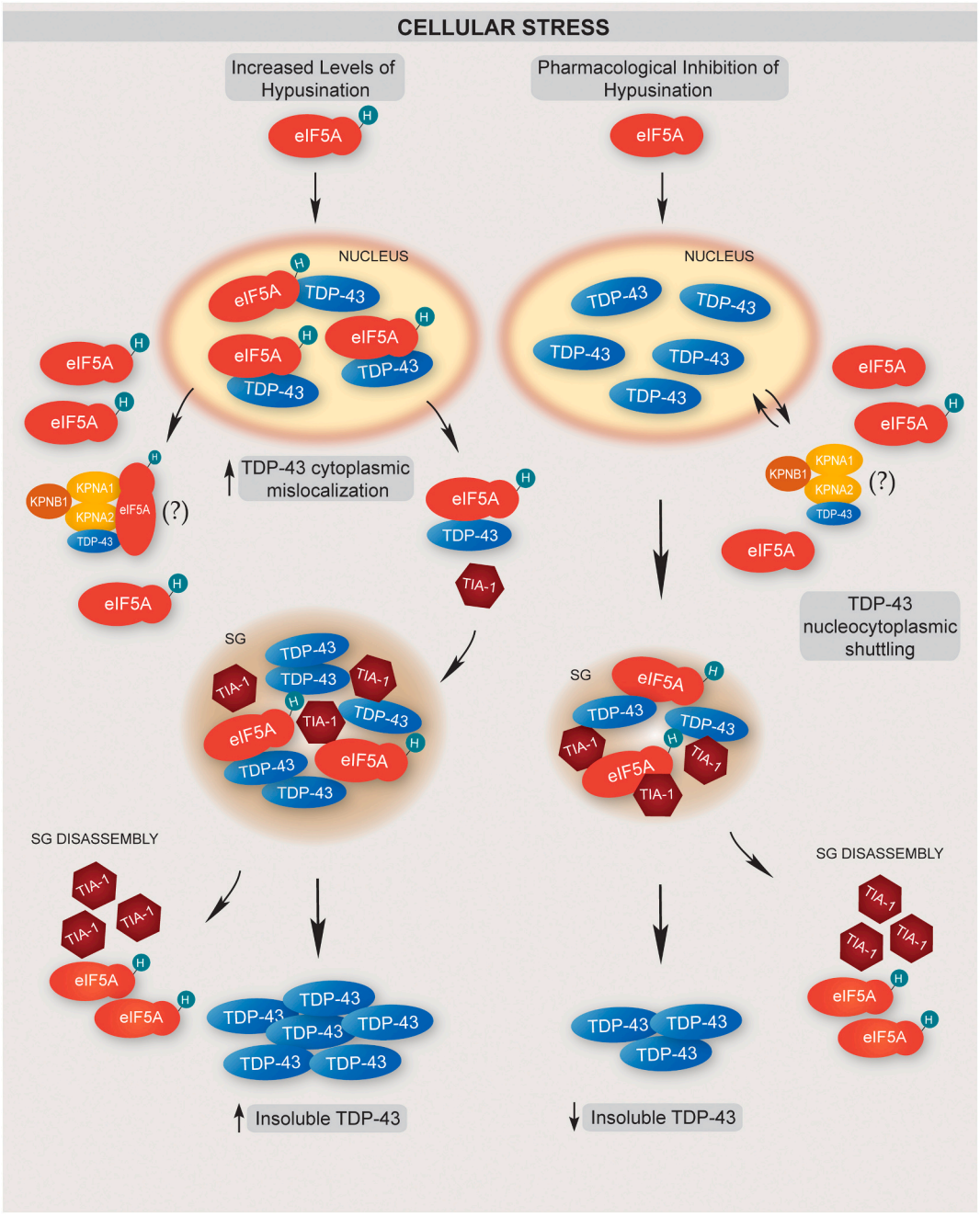

Fig. 9. Hypothetical model of the stress-induced nucleocytoplasmic transport and accumulation of TDP-43 via eIF5A^{HypK50}. In the cytoplasm, the interactions between cytoplasmic eIF5A^{HypK50} and TDP-43 strengthen, leading to the TDP-43 cytoplasmic retention and accumulation. We suggest that eIF5A^{HypK50} governs the accumulation of TDP-43 into TIA-1 positive stress granule, solidifying the role of eIF5A^{HypK50} as a regulator of the stress granule formation during cellular stress. Additionally, we find that eIF5A^{HypK50} is interacting with importins KPNA1/A2 and KPNB1 in the cytoplasm. We hypothesize that induced hypusination during stress promotes complex formations, leading to failed TDP-43 nuclear import and ultimately TDP-43 cytoplasmic sequestration. Subverting eIF5A^{HypK50} with novel pharmacological or genetic tools reduces cytoplasmic insoluble TDP-43 burden by recovering nucleocytoplasmic shuttling of TDP-43 as well as stabilize the stress granule dynamic.

membrane-less organelles contain a plethora of translation elongation initiation factors (eIF2, 3, 4, and 5) [50], small ribosomal subunits [51], and RBPs [52] shown to regulate the accumulation of numerous proteins and mRNA in SG. For instance, TDP-43 co-localization with SGs-specific RBPs TIA-1, eIF3 and PABP (polyadenylate-binding protein) was observed in both ALS and FTD brain [8–10,29,53] and in animal models [10,12]. In agreement with these studies, we reported co-localization of eIF5A^{HypK50} with TDP-43 in TIA-1 positive SGs upon cellular stress, an effect that was significantly reduced by GC7 treatment (Figs. 2 and 3). Interestingly, hypusinated eIF5A promotes SG assembly in an arsenite-induced cellular model and was efficiently reduced by GC7 treatment [27]. Similarly, we report here that reduced hypusination via GC7 significantly decreased SG number and density within the cell. More so, we demonstrated that GC7 treatment significantly decreased TDP-43 accumulation within the SG. This is in line with several studies raising the possibility of SG representing sites of early protein seeding and TDP-43 cytoplasmic aggregation [11]. To this point, we provided evidence that GC7 treatment significantly decreased cytoplasmic TDP-43 phosphorylation and aggregation, as measured in urea-soluble fraction (Fig. 6). However, our findings did not determine if SGs are a

contributing source of aggregated TDP-43 and require further investigation.

Studies suggest that the charged moiety of the exposed "hypusine loop" region, spanning Ser46-Ala54 ($SK^{47}TGK^{50}HGHA$), is important for eIF5A activity [54]. Indeed, we demonstrated that mutation of K47 and K50 to arginine (R) completely abolishes lysine acetylation and hypusination, respectively, which replicates the original findings from Park and colleagues [22,38,45]. More importantly, for the first time, we provide evidence that expression of $eIF5A^{K50R}$ mutant vastly reduced levels of total and pS409/410 TDP-43 in cells. Conversely, we show expression of $eIF5A^{K47R}$ maintained eIF5A hypusination and induced pTDP-43 in these cells (Fig. 4). Altogether, our data suggest that eIF5A hypusine vs. acetyl levels regulates TDP-43 cytoplasmic accumulation and aggregation. We also provide evidence that this regulatory pathway can be targeted by pharmacological and mutagenesis approaches against the hypusine loop moiety.

Notably, eIF5A hypusination has been proposed to regulate mRNA translation [55,56], nucleocytoplasmic shuttling of retroviral Rev., Rex RNA transport factors, and iNos mRNA processing [16,18]. For instance, eIF5A is involved in the CRM1/exportin cargo transport from the nucleus to the cytoplasm at the NPC [57]. Albeit our study did not focus on the translational regulation or the nucleocytoplasmic shuttling of $eIF5A^{HypK50}$, both proteomic enrichment data and biochemical analyzes provided evidence that NPC proteins, specifically importins KPNA1/2 KPNB1 and RanGTP were binding partners of $eIF5A^{HypK50}$ and were regulated by the hypusine levels. Indeed, we show that GC7 reduced KPNA1/2, B1, and RanGTP cytoplasmic expression levels, independent of SA-induced cellular stress (Figs. 1 and 4), which increased nuclear TDP-43 levels. The concentration of RanGTP in the nucleus and RanGDP in the cytosol forms a gradient harnessed by importins and exportins to provide nucleocytoplasmic transport [41–43]. This is of particular relevance since perturbed nucleocytoplasmic shuttling was recently found in diseases associated with mutations in the nuclear localization signals (NLSs) of FUS and in Heterogeneous nuclear ribonucleoprotein A1 (hnRNPA1) in ALS [47,58,59] and in chromosome 9 open reading frame 7 (C9ORF72) in both ALS and FTD cases [60–62]. Indeed, one study identified several NPC components within detergent-insoluble TDP-43 aggregates by proximity-dependent biotin identification (BioID) assay [63]. Others have recently demonstrated that cytoplasmic TDP-43 droplets recruit importin-alpha and Nup62, leading to mislocalization of RanGap1 and impaired nucleocytoplasmic transport, TDP-43 loss of function, and cell death [64]. Altogether, these studies strongly implicate pathology and transient stress to induce NPC dysfunction as a common mechanism for TDP-43 proteinopathy.

Here, we report mechanistic evidence that hypusination levels determine the interactions of eIF5A with TDP-43 and KPNA/B proteins. Based on our findings, we suggest that cytoplasmic interactions between TDP-43 and $eIF5A^{HypK50}$ are strengthened by cellular stress leading to the TDP-43 cytoplasmic retention and accumulation (Fig. 9). We also posit that $eIF5A^{HypK50}$ governs the accumulation of TDP-43 into TIA-1 positive SGs, solidifying the role of $eIF5A^{HypK50}$ as a regulator of the SG formation. Additionally, as the interactions between $eIF5A^{HypK50}$ and KPNA1/A2 and KPNB1 are dependent on the hypusine levels, we propose that induced hypusination promotes $eIF5A^{HypK50}$ interactions with KPNA1/2 and KPNB1, failing a proper TDP-43 nuclear import and ultimately contributing to TDP-43 cytoplasmic sequestration.

5. Conclusion

We show here that approaches against hypusination reduced insoluble TDP-43 levels by recovering nucleocytoplasmic shuttling of TDP-43 as well as stabilizing the SG dynamic. This study provides evidence on the role of the eIF5A hypusine loop as a unique target in common mechanisms of TDP-43 proteinopathies. Understanding the $eIF5A^{hypK50}$ governance of TDP-43 nucleocytoplasmic transport in disease-relevant models is crucial for future therapeutic approaches of TDP-43 pathogenesis.

Supplementary data to this article can be found online at https://doi.org/10.1016/j.bbadis.2020.165939.

CRediT authorship contribution statement

S.LS. performed immunocytochemistry, immunoprecipitation, Western blotting, cell treatments, microscopy, figure, and manuscript preparation. Z.Q. conducted the site-directed mutagenesis, Western blotting, and assisted with manuscript preparation. F.K. performed colocalization analysis, SUnSET experiment, Western blotting, Western blot analysis, microscopy, and figure preparation. A.M. conducted IPA and functional analyses. J.H. was involved in Western blots, urea soluble protein extractions, Western blot analysis, and figure preparation. A.L. N.S. conducted the stress granule counts. S.S. was involved in Western blotting and Western blot analysis. D.C. performed the mass spectroscopy. D.L. assisted in experimental design and manuscript revision. M.L.B.S. conceived the experimental plan, provided funding, assisted with data interpretation, figure and manuscript preparation, and provided reviewing and editing of the final revision.

Declaration of competing interest

The authors declare that they have no known competing financial interests or personal relationships that could have appeared to influence the work reported in this paper.

Acknowledgments

This work was supported by the College of Pharmacy Start-up Funds and COP New Investigator Seed Grant, , University of South Florida FL, USA.

References

[1] M. Grossman, Frontotemporal dementia: a review, J. Int. Neuropsychol. Soc. 8 (4) (2002) 566–583.
[2] I.R. Mackenzie, R. Rademakers, M. Neumann, TDP-43 and FUS in amyotrophic lateral sclerosis and frontotemporal dementia, Lancet Neurol. 9 (10) (2010) 995–1007.
[3] S.C. Ling, et al., ALS-associated mutations in TDP-43 increase its stability and promote TDP-43 complexes with FUS/TLS, Proc. Natl. Acad. Sci. U. S. A. 107 (30) (2010) 13318–13323.
[4] P.T. Nelson, et al., Limbic-predominant age-related TDP-43 encephalopathy (LATE): consensus working group report, Brain 142 (6) (2019) 1503–1527.
[5] T.J. Cohen, V.M. Lee, J.Q. Trojanowski, TDP-43 functions and pathogenic mechanisms implicated in TDP-43 proteinopathies, Trends Mol. Med. 17 (11) (2011) 659–667.
[6] A. Shiga, et al., Alteration of POLDIP3 splicing associated with loss of function of TDP-43 in tissues affected with ALS, PLoS One 7 (8) (2012) e43120.
[7] A. Cortese, et al., Widespread RNA metabolism impairment in sporadic inclusion body myositis TDP43-proteinopathy, Neurobiol. Aging 35 (6) (2014) 1491–1498.
[8] D. Dormann, et al., Proteolytic processing of TAR DNA binding protein-43 by caspases produces C-terminal fragments with disease defining properties independent of progranulin, J. Neurochem. 110 (3) (2009) 1082–1094.
[9] K. Volkening, et al., Tar DNA binding protein of 43 kDa (TDP-43), 14-3-3 proteins and copper/zinc superoxide dismutase (SOD1) interact to modulate NFL mRNA stability. Implications for altered RNA processing in amyotrophic lateral sclerosis (ALS), Brain Res. 1305 (2009) 168–182.
[10] L. Liu-Yesucevitz, et al., Tar DNA binding protein-43 (TDP-43) associates with stress granules: analysis of cultured cells and pathological brain tissue, PLoS One 5 (10) (2010) e13250.
[11] H.J. Kim, et al., Therapeutic modulation of eIF2alpha phosphorylation rescues TDP-43 toxicity in amyotrophic lateral sclerosis disease models, Nat. Genet. 46 (2) (2014) 152–160.
[12] A.C. Elden, et al., Ataxin-2 intermediate-length polyglutamine expansions are associated with increased risk for ALS, Nature 466 (7310) (2010) 1069–1075.
[13] M.H. Park, et al., Functional significance of eIF5A and its hypusine modification in eukaryotes, Amino Acids 38 (2) (2010) 491–500.
[14] M.H. Park, The post-translational synthesis of a polyamine-derived amino acid, hypusine, in the eukaryotic translation initiation factor 5A (eIF5A), J. Biochem. 139 (2) (2006) 161–169.
[15] E.C. Wolff, et al., Posttranslational synthesis of hypusine: evolutionary progression and specificity of the hypusine modification, Amino Acids 33 (2) (2007) 341–350.
[16] W. Hofmann, et al., Cofactor requirements for nuclear export of Rev response element (RRE)- and constitutive transport element (CTE)-containing retroviral RNAs.

An unexpected role for actin, J. Cell Biol. 152 (5) (2001) 895–910.
[17] D. Zuk, A. Jacobson, A single amino acid substitution in yeast eIF-5A results in mRNA stabilization, EMBO J. 17 (10) (1998) 2914–2925.
[18] B. Maier, et al., The unique hypusine modification of eIF5A promotes islet beta cell inflammation and dysfunction in mice, J. Clin. Invest. 120 (6) (2010) 2156–2170.
[19] R.D. Robbins, et al., Inhibition of deoxyhypusine synthase enhances islet {beta} cell function and survival in the setting of endoplasmic reticulum stress and type 2 diabetes, J. Biol. Chem. 285 (51) (2010) 39943–39952.
[20] J. Jakus, et al., Features of the spermidine-binding site of deoxyhypusine synthase as derived from inhibition studies. Effective inhibition by bis- and mono-guanylated diamines and polyamines, J. Biol. Chem. 268 (18) (1993) 13151–13159.
[21] S.B. Lee, et al., Inactivation of eukaryotic initiation factor 5A (eIF5A) by specific acetylation of its hypusine residue by spermidine/spermine acetyltransferase 1 (SSAT1), Biochem. J. 433 (1) (2011) 205–213.
[22] S.B. Lee, et al., The effect of hypusine modification on the intracellular localization of eIF5A, Biochem. Biophys. Res. Commun. 383 (4) (2009) 497–502.
[23] H. Sievert, et al., Protein-protein-interaction network organization of the hypusine modification system, Mol. Cell. Proteomics 11 (11) (2012) 1289–1305.
[24] A. Mandal, S. Mandal, M.H. Park, Global quantitative proteomics reveal up-regulation of endoplasmic reticulum stress response proteins upon depletion of eIF5A in HeLa cells, Sci. Rep. 6 (2016) 25795.
[25] M. Budini, et al., TDP-43 loss of cellular function through aggregation requires additional structural determinants beyond its C-terminal Q/N prion-like domain, Hum. Mol. Genet. 24 (1) (2015) 9–20.
[26] Y. Nishiki, et al., Characterization of a novel polyclonal anti-hypusine antibody, Springerplus 2 (2013) 421.
[27] C.H. Li, et al., eIF5A promotes translation elongation, polysome disassembly and stress granule assembly, PLoS One 5 (4) (2010) e9942.
[28] B.S. Johnson, et al., TDP-43 is intrinsically aggregation-prone, and amyotrophic lateral sclerosis-linked mutations accelerate aggregation and increase toxicity, J. Biol. Chem. 284 (30) (2009) 20329–20339.
[29] A. Aulas, C. Vande Velde, Alterations in stress granule dynamics driven by TDP-43 and FUS: a link to pathological inclusions in ALS? Front. Cell. Neurosci. 9 (2015) 423.
[30] L.I. Binder, et al., Tau, tangles, and Alzheimer's disease, Biochim. Biophys. Acta 1739 (2–3) (2005) 216–223.
[31] M.C. Gao, et al., Intelligence in Williams Syndrome is related to STX1A, which encodes a component of the presynaptic SNARE complex, PLoS One 5 (4) (2010) e10292.
[32] K. Frid, et al., Aggregation of MBP in chronic demyelination, Ann. Clin. Transl. Neurol. 2 (7) (2015) 711–721.
[33] I. Corradini, et al., SNAP-25 in neuropsychiatric disorders, Ann. N. Y. Acad. Sci. 1152 (2009) 93–99.
[34] C. Colombrita, et al., TDP-43 is recruited to stress granules in conditions of oxidative insult, J. Neurochem. 111 (4) (2009) 1051–1061.
[35] Y. Khalfallah, et al., TDP-43 regulation of stress granule dynamics in neurodegenerative disease-relevant cell types, Sci. Rep. 8 (1) (2018) 7551.
[36] H.A. Kang, J.W. Hershey, Effect of initiation factor eIF-5A depletion on protein synthesis and proliferation of Saccharomyces cerevisiae, J. Biol. Chem. 269 (6) (1994) 3934–3940.
[37] E.K. Schmidt, et al., SUnSET, a nonradioactive method to monitor protein synthesis, Nat. Methods 6 (4) (2009) 275–277.
[38] M. Ishfaq, et al., Acetylation regulates subcellular localization of eukaryotic translation initiation factor 5A (eIF5A), FEBS Lett. 586 (19) (2012) 3236–3241.
[39] B. Cautain, et al., Components and regulation of nuclear transport processes, FEBS J. 282 (3) (2015) 445–462.
[40] M. Soniat, Y.M. Chook, Nuclear localization signals for four distinct karyopherin-beta nuclear import systems, Biochem. J. 468 (3) (2015) 353–362.
[41] H.J. Kim, J.P. Taylor, Lost in transportation: nucleocytoplasmic transport defects in ALS and other neurodegenerative diseases, Neuron 96 (2) (2017) 285–297.
[42] M. Raices, M.A. D'Angelo, Nuclear pore complex composition: a new regulator of tissue-specific and developmental functions, Nat. Rev. Mol. Cell Biol. 13 (11) (2012) 687–699.
[43] F. Melchior, Ran GTPase cycle: oOne mechanism – two functions, Curr. Biol. 11 (7) (2001) R257–R260.
[44] M. Neumann, Molecular neuropathology of TDP-43 proteinopathies, Int. J. Mol. Sci. 10 (1) (2009) 232–246.
[45] J.H. Park, et al., Production of active recombinant eIF5A: reconstitution in E.coli of eukaryotic hypusine modification of eIF5A by its coexpression with modifying enzymes, Protein Eng. Des. Sel. 24 (3) (2011) 301–309.
[46] O.D. King, A.D. Gitler, J. Shorter, The tip of the iceberg: RNA-binding proteins with prion-like domains in neurodegenerative disease, Brain Res. 1462 (2012) 61–80.
[47] J. Gal, et al., Nuclear localization sequence of FUS and induction of stress granules by ALS mutants, Neurobiol Aging 32 (12) (2011) 2323 (e27-40).
[48] M. Kamelgarn, et al., ALS mutations of FUS suppress protein translation and disrupt the regulation of nonsense-mediated decay, Proc. Natl. Acad. Sci. U. S. A. 115 (51) (2018) E11904–E11913.
[49] P.E. Ash, et al., Pathological stress granules in Alzheimer's disease, Brain Res. 1584 (2014) 52–58.
[50] P. Anderson, N. Kedersha, RNA granules: post-transcriptional and epigenetic modulators of gene expression, Nat. Rev. Mol. Cell Biol. 10 (6) (2009) 430–436.
[51] N.G. Farny, N.L. Kedersha, P.A. Silver, Metazoan stress granule assembly is mediated by P-eIF2alpha-dependent and -independent mechanisms, RNA 15 (10) (2009) 1814–1821.
[52] N. Gilks, et al., Stress granule assembly is mediated by prion-like aggregation of TIA-1, Mol. Biol. Cell 15 (12) (2004) 5383–5398.
[53] L. McGurk, et al., Poly-A binding protein-1 localization to a subset of TDP-43 inclusions in amyotrophic lateral sclerosis occurs more frequently in patients harboring an expansion in C9orf72, J. Neuropathol. Exp. Neurol. 73 (9) (2014) 837–845.
[54] V.S. Cano, et al., Mutational analyses of human eIF5A-1–identification of amino acid residues critical for eIF5A activity and hypusine modification, FEBS J. 275 (1) (2008) 44–58.
[55] A. Henderson, J.W. Hershey, The role of eIF5A in protein synthesis, Cell Cycle 10 (21) (2011) 3617–3618.
[56] P. Saini, et al., Hypusine-containing protein eIF5A promotes translation elongation, Nature 459 (7243) (2009) 118–121.
[57] C. Elfgang, et al., Evidence for specific nucleocytoplasmic transport pathways used by leucine-rich nuclear export signals, Proc. Natl. Acad. Sci. U. S. A. 96 (11) (1999) 6229–6234.
[58] D. Dormann, et al., ALS-associated fused in sarcoma (FUS) mutations disrupt Transportin-mediated nuclear import, EMBO J. 29 (16) (2010) 2841–2857.
[59] Q. Liu, et al., Whole-exome sequencing identifies a missense mutation in hnRNPA1 in a family with flail arm ALS, Neurology 87 (17) (2016) 1763–1769.
[60] S. Boeynaems, et al., Inside out: the role of nucleocytoplasmic transport in ALS and FTLD, Acta Neuropathol. 132 (2) (2016) 159–173.
[61] A. Jovicic, et al., Modifiers of C9orf72 dipeptide repeat toxicity connect nucleocytoplasmic transport defects to FTD/ALS, Nat. Neurosci. 18 (9) (2015) 1226–1229.
[62] K. Zhang, et al., The C9orf72 repeat expansion disrupts nucleocytoplasmic transport, Nature 525 (7567) (2015) 56–61.
[63] C.C. Chou, et al., TDP-43 pathology disrupts nuclear pore complexes and nucleocytoplasmic transport in ALS/FTD, Nat. Neurosci. 21 (2) (2018) 228–239.
[64] F. Gasset-Rosa, et al., Cytoplasmic TDP-43 De-mixing independent of stress granules drives inhibition of nuclear import, loss of nuclear TDP-43, and cell death, Neuron 102 (2) (2019) 339–357 (e7).
[65] Y. Benjamini, Y. Hechtlinger, Discussion: an estimate of the science-wise false discovery rate and applications to top medical journals by Jager and Leek, Biostatistics 15 (1) (2014) 13–16 (discussion 39-45).